Investigation of the structural, electronic, mechanical, and optical properties of $X_2MgH_6\left(X=Ba,Sr\right)$ hydrides for hydrogen storage

K. Sabir¹, K. El-Achouri¹, Lahoucine Bahmad², O. El Fatni¹

¹LPHE-MS, Faculty of Science, Mohammed V University, Rabat, Morocco
²Laboratory of Condensed Matter and Interdisciplinary Sciences (LaMCScI), Faculty of Science, Mohammed V University, Rabat, Morocco

Article Info

Article history:

Received Jan 31, 2025 Revised Apr 12, 2025 Accepted Jun 1, 2025

Keywords:

Density functional theory Gravimetric hydrogen storage capacity Hydrogen storage Mechanical properties Perovskite

ABSTRACT

This study examines the structural, electronic, mechanical, and optical characteristics of X_2MgH_6 hydrides (where X=Ba, Sr) for hydrogen storage applications. These compounds, featuring a double perovskite crystal structure, show significant promise for hydrogen storage owing to their thermodynamic stability and robust mechanical attributes. First principles calculations using density functional theory (DFT) indicate negative formation enthalpies, verifying their thermodynamic stability. The electronic characteristics, such as band gaps and density of states, affect the materials' electrical conductivity and chemical reactivity. Mechanical evaluations using elastic constants and modulus data demonstrate that Sr_2MgH_6 possesses higher strength and stiffness compared to Ba_2MgH_6 . Furthermore, optical traits like ultraviolet (UV) absorption and visible light reflectivity point to possible uses in optoelectronic and photonic technologies. This research advances the comprehension of complex hydrides and supports the advancement of hydrogen storage systems, essential for the global shift toward sustainable energy.

This is an open access article under the **CC BY-SA** license.



Corresponding Author:

Lahoucine Bahmad

Laboratory of Condensed Matter and Interdisciplinary Sciences (LaMCScI), Faculty of Science

Mohammed V University

Rabat, Morocco

Email: bahmad@um5r.ac.ma

1. INTRODUCTION

The escalating energy and environmental crises of the 21st century have intensified global efforts to transition toward sustainable and low carbon energy systems [1], [2]. Anthropogenic greenhouse gas emissions, predominantly from fossil fuel combustion, remain the principal driver of planetary warming and its cascading impacts on ecological stability and socio-economic resilience [3], [4]. In response, hydrogen (H₂) has emerged as a pivotal element for decarbonizing hard-to-abate sectors, including heavy-duty transportation, industrial processes, and grid-scale energy storage [5], [6]. Its inherent properties-zero greenhouse gas emissions upon utilization, high gravimetric energy density (120–140 MJ/kg), and adaptability as an energy carrier position it as a cornerstone of the sustainable energy transition [2], [7], [8].

However, the widespread implementation of hydrogen-based technologies faces multifaceted barriers, including inefficient production pathways, material compatibility challenges, and underdeveloped distribution infrastructure [9]. Currently, most hydrogen production relies on carbon-intensive processes such

as steam methane reforming [10]. For hydrogen to fully contribute to the energy transition, cleaner production methods, such as water electrolysis powered by renewable energy, must be developed [11], [12]. Additionally, hydrogen storage and transportation present significant technical and economic challenges [13], [14]. Conventional storage methods, including high-pressure tanks and cryogenic liquid storage, have limitations in terms of cost, safety, and efficiency [6], [15]. Hence, to achieve these targets, significant technological development is needed to improve the energy density, safety, and efficiency of hydrogen storage and distribution systems [16].

However, the opportunity for reversible hydrogen storage has led to increasing interest in promising metal hydrides, specifically complex hydrides belonging to the X_2MgH_6 family of compounds (X=Ba, Sr) [1], [17]. These materials show interesting potential for solid-state hydrogen storage as they have a specific crystalline structure for adsorption [18], [19]. Materials has recently studied double perovskite materials and hydrides that include ABH₃ or A_2BH_6 as a result of their enormous storage capacities [20], [21]. Examples of gravimetric densities obtained from the study of hydrides, such as NaXH₃ (X=Ti, Cu) or K₂SiH₆, demonstrate excellent gravimetric densities [22]–[24]. Mainly driven by theoretical approaches, especially DFT, which is important in investigating intrinsic properties of materials and assisting their design in optimization [25], [26].

In this study, ab initio calculations based on DFT were performed to analyze the structural, electronic, mechanical, and optical properties of X_2MgH_6 hydrides (X=Ba, Sr). The goals are to describe the hydrolysis behavior that sustainably facilitates their performance as hydrogen storage materials, and to address the obstacles that these materials would face if implemented in real industrial settings. The paper is divided into three sections: an introduction to DFT and the computational parameters which we employed, an in-depth analysis of the properties of the hydrides, and a discussion the results and their implications on hydrogen storage.

This research is intended to help deepen the understanding of complex hydrides and further develop new approaches to hydrogen storage problems. Such advancements could enable major breakthroughs in materials science and energy engineering, solidifying hydrogen as a cornerstone of the global energy transition.

2. METHOD

In this work, we used DFT, with implementation in the Cambridge serial total energy package (CASTEP), to calculate the physical properties of the complex hydrides X_2MgH_6 (X=Ba, Sr) [27], [28]. Ultrasoft pseudopotentials (USPP) were used to model the interactions between electrons and ions, in order to adequately represent the interactions between atomic nuclei and valence electrons [8].

Among the four elements analyzed in this research are barium (Ba), strontium (Sr), magnesium (Mg), and hydrogen (H) [22], [29]. The selected materials are from the X_2 Mg H_6 family, where X=Ba, Sr. For an accurate description of the electronic interactions, we used Perdew burke ernzerhof (PBE) functional in the generalized gradient approximation (GGA) [30], [31]. We selected the (super)cell approach owing to its demonstrated capacity at predicting accurate estimates of structural and electronic properties for complex hydrides, while maintaining a balance between accuracy and computational efficiency and can do so with a gradual compromise between accuracy and run time.

We performed the calculations using a plane-wave basis set with an energy cut-off of 600 eV which provides a trade-off between accuracy and computational cost. Similar energy cut-off has been shown to give good convergence of the structural and energetic properties for similar systems. A $(10\times10\times10)$ Monkhorst-pack k-point mesh was used to generate the k-point, providing affording an optimal coverage of the reciprocal space [24], [32].

Geometric optimization was performed using rigorous convergence parameters to ensure structural accuracy: energy tolerance of 1×10^{-6} eV/atom, maximum residual force of 0.01 eV/Å, and maximum ionic displacement of 1×10^{-4} Å. These criteria guarantee that the optimized structures correspond to local energy minima, ensuring the reliability of subsequent analyses of electronic and mechanical properties. All simulations were executed under idealized conditions (0K, 0GPa) to isolate intrinsic material behavior, eliminating thermal fluctuations and external pressure effects.

Mechanical properties were evaluated via the stress-strain method within a first-principles framework, enabling the determination of elastic stiffness constants (C_{ij} [33], [34]. This approach quantifies the materials' resistance to deformation and provides critical insights into their intrinsic mechanical response, essential for assessing structural stability and applicability in hydrogen storage systems.

3. RESULTS AND DISCUSSIONS

3.1. Structural and hydrogen storage properties

The X_2 Mg H_6 (X=Ba, Sr) hydrides adopt a double perovskite-type framework, crystallizing within a trigonal lattice system (space group P 3 m1, No. 164) In this structure, Mg²⁺ cations are octahedrally coordinated with six hydrogen atoms, forming [MgH 6]⁴⁻ complexes, while the X²⁺ (Ba²⁺ or Sr²⁺) cations occupy the central cavity of the unit cell, acting as charge-balancing counter-ions to stabilize the lattice Figure 1 [35], [36].

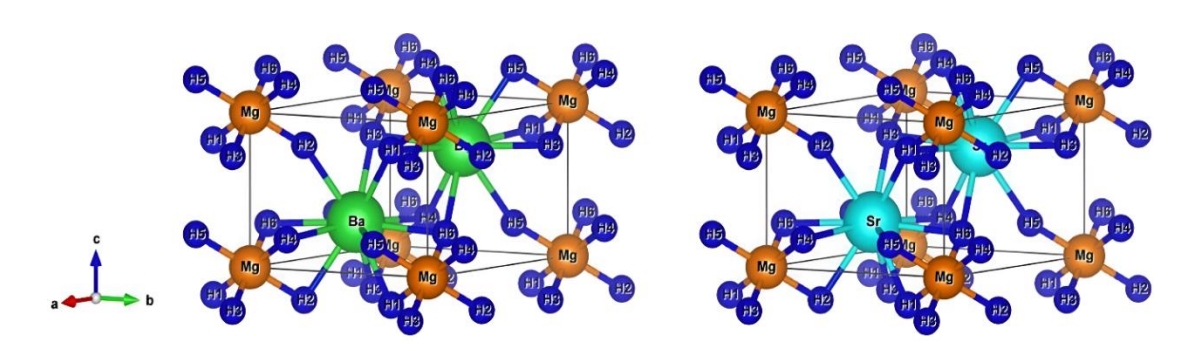


Figure 1. The crystal structure of X_2 Mg H_6 (X=Ba, Sr) double perovskite type hydrides

Structural optimization reveals distinct lattice parameters for $Ba_2\text{Mg}H_6$ (a=5.7178 Å, c=4.5383 Å) and $Sr_2\text{Mg}H_6$ (a=5.4754 Å, c=4.1885 Å), directly correlated with the ionic radii of the X^{2+} cations. The larger Ba^{2+} ion (1.35 Å) induces a more expanded lattice compared to Sr^{2+} (1.18 Å), consistent with the structural tolerance of perovskite-derived materials, where cation size dictates lattice volume to accommodate ionic packing [24], [35].

The ionic radius of X^{2+} governs both structural stability and hydrogen storage dynamics. The larger Ba^{2+} generates an open framework, potentially enhancing hydrogen diffusion kinetics but compromising mechanical robustness under compressive stress. Conversely, the smaller Sr^{2+} promotes a compact lattice, improving mechanical integrity at the expense of reduced hydrogen mobility.

The stability of the crystal structure is a key parameter for hydrogen storage applications. To assess this stability, the energy-volume curve was computed, as illustrated in Figure 2. The energy-volume relationship provides insights into the thermodynamic stability of the materials, where the minimum energy corresponds to the equilibrium lattice volume. Both Ba_2MgH_6 and Sr_2MgH_6 exhibit well-defined minima, confirming their thermodynamic stability at their respective equilibrium volumes. However, subtle differences in the curvature of these plots suggest that Sr_2MgH_6 may exhibit slightly higher resistance to volume changes under external pressure, which could be advantageous for applications requiring enhanced mechanical robustness.

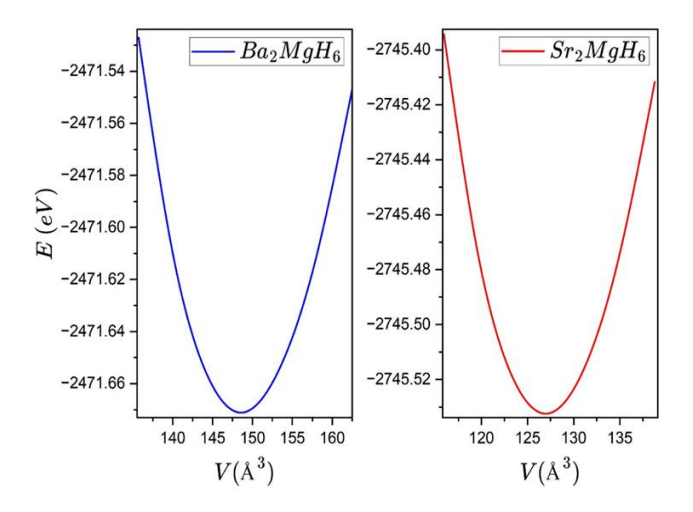


Figure 2. Calculated energy-volume curves for double perovskite-type hydrides X_2MgH_6 (X=Ba, Sr)

3.2. Thermodynamic stability

The thermodynamic stability of the compounds was assessed by calculating their formation enthalpies [37]. For Ba_2MgH_6 , the formation enthalpy is -2870.76 KJ/mol, whereas for Sr_2MgH_6 , it is -2809.10 KJ/mol. The formation energy (ΔH_f) was determined using as (1) [38].

$$\Delta H_f(X_2 MgH_6) = [E_{total}(X_2 MgH_6) - 2E_s(X) - E_s(Mg) - 6E_s(H)]$$
(1)

The results indicate that Ba_2MgH_6 exhibits slightly higher thermodynamic stability due to its more negative formation enthalpy, suggesting greater overall stability under various conditions. Both compounds have negative formation enthalpies, confirming their thermodynamic stability and favorable under standard conditions.

Thermodynamic stability is a key parameter for hydrogen storage applications, as it directly affects the durability and safety of materials over the long term [39]. A strongly negative formation enthalpy, as observed for Ba_2MgH_6 and Sr_2MgH_6 , indicates that these materials are thermodynamically favorable and unlikely to decompose spontaneously under normal conditions. This is essential for hydrogen storage systems, where long-term chemical stability is required to prevent hydrogen leakage or material degradation. However, thermodynamic stability must be balanced with the ease of hydrogen release. Although Ba_2MgH_6 is slightly more stable than Sr_2MgH_6 this increased stability could make hydrogen desorption more difficult, requiring higher temperatures or stricter conditions to release the stored hydrogen. In contrast, Sr_2MgH_6 , being slightly less stable, might allow for easier hydrogen release, which is beneficial for practical applications where controlled and rapid hydrogen desorption is necessary.

The double perovskite structure of these hydrides enhances their potential for long-term hydrogen storage applications [40], [41]. This specific crystalline arrangement provides high mechanical and chemical stability, which is crucial for withstanding repeated hydrogen absorption-desorption cycles without significant degradation. Additionally, the thermodynamic stability of these materials suggests that they can maintain their structural integrity over extended periods, even in environments subject to temperature or pressure fluctuations [42].

3.3. Gravimetric storage capacity

The gravimetric hydrogen storage capacity was calculated using (2) [15], [17]:

$$CWt\% = \frac{\frac{H}{M}m_{H2}}{m_{Host} + (\frac{H}{M})m_{H2}} *100\%$$
 (2)

where:

 $\frac{H}{M}$: Hydrogen/metal molar ratio

 m_{H2} : Molar mass of hydrogen (2.016 g/mol)

 m_{Host} : Molar mass of the host material (in g/mol)

This formula provides a quantitative measure of a material's hydrogen storage efficiency, taking into account both the amount of hydrogen stored relative to the mass of the host material, and the chemical composition of the system. Gravimetric storage capacity is essential for assessing the viability of a material for hydrogen storage, particularly in applications requiring high energy density. A high gravimetric storage capacity indicates a more efficient material, enabling more energy to be stored per unit mass, which is crucial for portable and automotive applications where space and weight are limited. By analyzing this capacity, it is possible to identify promising hydrides for more efficient and sustainable hydrogen storage solutions, paving the way for advances in clean energy technologies.

For $Ba_2 \text{Mg}H_6$, this ratio is 1.33%, while for $Sr_2 \text{Mg}H_6$, it reaches 1.98%, which is a 49% improvement compared to its barium counterpart. Although these values are still lower than those of classical hydrides like $\text{Mg}H_2$ (7.6%) or NaAlH_4 (5.6%), the $X_2 \text{Mg}H_6$ hydrides (X=Ba, Sr) stand out due to their double perovskite structure, offering exceptional mechanical and thermodynamic stability, as well as low toxicity [18], [19]. Unlike $\text{LaNi}_5 \text{H}_6$ (1.5%), which has risks associated with lanthanum, or $\text{Mg}H_2$, which requires desorption temperatures higher than 300 °C, these materials allow for safe storage at room temperature [20], [21]. However, their practical application is limited by cryogenic desorption temperatures (~21–22 K), requiring innovative approaches such as doping, Nano structuring, or integration into porous matrices (MOFs) to improve their kinetics [22], [43]. Despite these challenges, their safety profile and durability make them promising candidates for niche applications where long-term reliability outweighs storage density, paving the way for future research focused on optimizing their desorption properties [44]. Compared to these

materials, Ba_2MgH_6 and Sr_2MgH_6 exhibit relatively low storage capacities. However, their double perovskite structure could offer advantages in terms of stability and storage conditions. Moreover, their low toxicity and thermodynamic stability can offset their moderate storage capacity depending on the targeted applications.

3.4. Hydrogen desorption temperature

The hydrogen desorption temperature (T_{des}) for both compounds was calculated using (3) [45].

$$T_{des} = \frac{-\Delta H_f}{\Delta S} \tag{3}$$

The desorption temperature, where ΔH_f represents the enthalpy of formation and ΔS represents the change in entropy, provides valuable insights into the energy required to release hydrogen from the material. It plays a crucial role in evaluating the practical feasibility of these hydrides for hydrogen storage applications.

In the context of hydrogen storage, a material's desorption temperature is directly related to its ability to release stored hydrogen under controlled conditions. A lower desorption temperature is desirable for applications requiring efficient hydrogen release at moderate temperatures, making the material more suitable for use in fuel cells or other energy systems. By calculating the desorption temperature, we gain important information about the material's thermodynamic properties, specifically its stability and the energy barriers involved in hydrogen release.

Including the desorption temperature in this study allows for a comprehensive understanding of the storage and release characteristics of $Ba_2 \text{Mg}H_6$ and $Sr_2 \text{Mg}H_6$. It provides an essential parameter to guide further optimization of these materials for practical hydrogen storage applications, especially for systems that demand rapid desorption at low temperatures. This calculation, along with the evaluation of the materials' mechanical, structural, and thermodynamic properties, contributes to a holistic assessment of their potential for use in real-world hydrogen storage technologies.

The desorption temperature of the $Ba_2 \text{Mg}H_6$ material is 21.96 K, while for $Sr_2 \text{Mg}H_6$, it is slightly lower at 21.49 K. Although these temperatures are physically plausible, they are too low for commercial hydrogen storage applications, which typically require operating temperatures between 298 K and 473 K (25–200 °C) [46], [47]. These cryogenic values suggest that $Ba_2 \text{Mg}H_6$ and $Sr_2 \text{Mg}H_6$ may be more suitable for cryogenic applications, such as liquid hydrogen storage for aerospace, where extremely low temperatures can be maintained. However, for ambient temperature applications, structural modifications or innovative approaches would be necessary to raise the desorption temperature and make these materials viable for commercial use. For example, further studies could explore the effect of pressure on hydrogen desorption by adjusting pressure conditions to shift the thermodynamic equilibrium and increase the desorption temperature to more practical levels [48], [49]. Additionally, strategies such as doping with catalytic elements (e.g., Ti, Ni) or integrating into porous matrices (e.g., MOFs) could be considered to improve desorption properties [50]–[52]. With these modifications, $Ba_2 \text{Mg}H_6$ and $Sr_2 \text{Mg}H_6$ could be adapted for ambient temperature applications, such as stationary storage or hydrogen vehicle systems, paving the way for future research aimed at optimizing their performance for practical uses.

3.5. Electronic properties

The electronic properties of X_2 Mg H_6 (X=Ba, Sr) hydrides critically govern their functionality as hydrogen storage materials, with distinct disparities in band structures and density of states (DOS) directly influencing their operational performance. Band structure analysis Figures 3(a) and 3(b) reveals a narrower indirect bandgap of 2.695 eV for Sr_2 Mg H_6 enabling enhanced charge carrier mobility across valence and conduction bands. This electronic configuration facilitates improved electrical conductivity, rendering the material advantageous for high-performance electronic applications. Conversely, Ba_2 Mg H_6 exhibits a wider indirect bandgap of 2.907 eV, characteristic of perovskite-type hydrides [32]. Which confers intrinsic electronic stability and insulating behavior. Such properties are particularly beneficial for applications demanding structural integrity and resistance to degradation during repeated hydrogen absorption/desorption cycles. Complementary DOS profiles (Figure 4) further highlight a pronounced DOS near the Fermi level in Sr_2 Mg H_6 [33]. Correlating with its heightened electronic reactivity and conductivity compared to Ba_2 Mg H_6 . These findings underscore the interplay between electronic structure and functional performance, providing critical insights for tailoring hydride materials to specific energy storage requirements.

This observation indicates a stronger interaction with hydrogen, facilitating its adsorption through increased electron availability to form chemical bonds. A higher DOS near the Fermi level is often associated with improved conductivity and reactivity, which is essential for hydrogen storage applications where

efficient adsorption is required. This enhanced interaction is crucial for improving the efficiency of hydrogen absorption and desorption processes.

The elevated total density of states (TDOS) near the Fermi level in Sr_2MgH_6 directly correlates with enhanced hydrogen interaction, as increased electron availability facilitates stronger chemical bond formation during adsorption. A high DOS near the Fermi level is a hallmark of materials with superior charge transfer kinetics and reactivity, both of which are critical for efficient hydrogen storage systems requiring rapid adsorption/desorption cycles. Figure 5 further elucidates this mechanism through partial density of states (PDOS) analysis, which highlights the dominant contribution of p-orbitals near the Fermi level. This p-orbital dominance governs electronic transitions and chemical bonding with hydrogen, directly modulating storage capacity and desorption kinetics. The pronounced role of p-orbitals underscores their significance in tailoring electronic structures for optimized reactivity and conductivity in hydride systems.

Collectively, the electronic properties of $Ba_2 \text{Mg}H_6$ and $Sr_2 \text{Mg}H_6$ including bandgap energetics (Figure 3), TDOS profiles (Figure 4), and p-orbital contributions (Figure 5) demonstrate their tailored suitability for hydrogen storage applications. While $Sr_2 \text{Mg}H_6$'s narrower bandgap and high DOS enable rapid hydrogen kinetics, $Ba_2 \text{Mg}H_6$'s wider bandgap ensures structural stability during cycling. These insights provide a foundational framework for engineering hydrides with balanced reactivity and durability, advancing the development of next-generation materials for sustainable energy storage. Such optimizations are pivotal for addressing global energy challenges through improved hydrogen economy technologies.

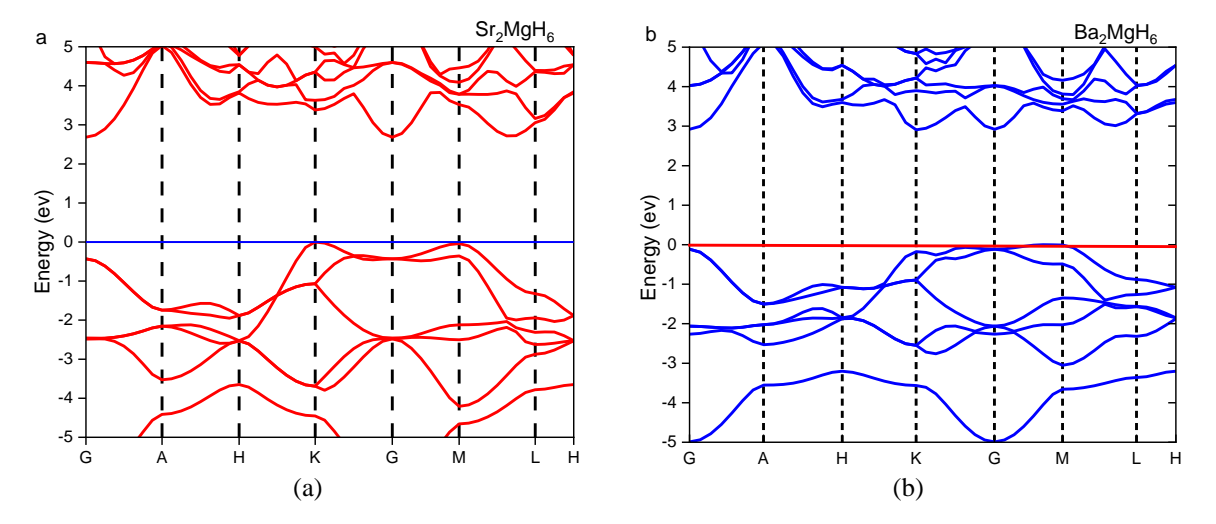


Figure 3. Calculated electronic band structures of X_2MgH_6 (X=Ba, Sr): (a) Sr_2MgH_6 and (b) Ba_2MgH_6

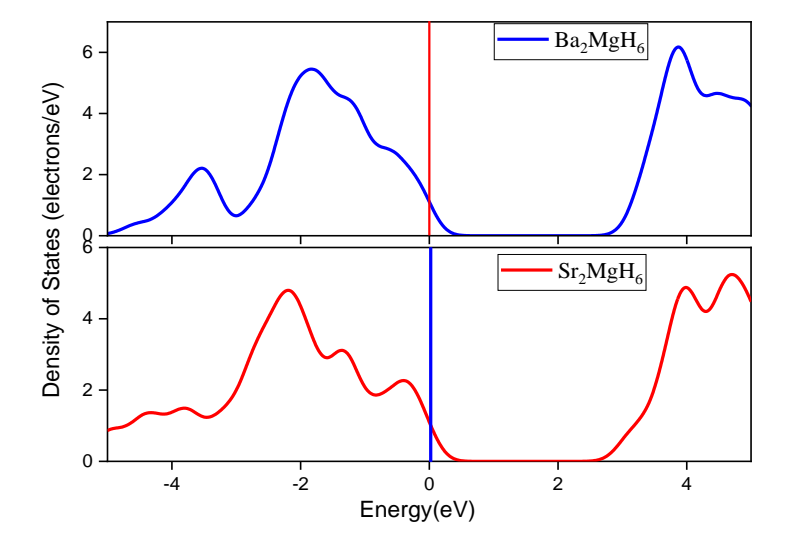


Figure 4. TDOS for X_2MgH_6 (X=Ba, Sr)

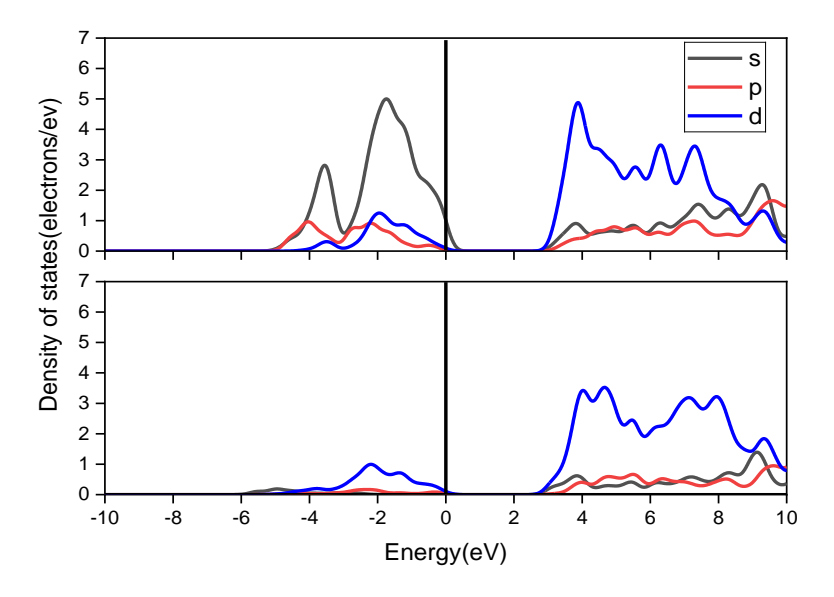


Figure 5. PDOS for X_2MgH_6 (X=Ba, Sr)

3.6. Mechanical properties

The mechanical properties of Ba_2MgH_6 and Sr_2MgH_6 hydrides are essential for assessing their robustness and durability in hydrogen storage applications. An in-depth analysis of the elastic constants and mechanical module, presented in Tables 1 and 2, as well as the graphical representations in Figures 6 and 7, reveals significant differences between these two materials.

Table 1 shows the elastic constants calculated for Ba_2MgH_6 and Sr_2MgH_6 . Sr_2MgH_6 stands out for its higher compressive strength, with a C_{11} constant of 95.76 GPa, compared with 84.83 GPa for Ba_2MgH_6 . This difference indicates that Sr_2MgH_6 is better able to resist deformation under load, a crucial factor for applications requiring high mechanical strength. In addition, Sr_2MgH_6 has a young modulus (Y) of 87.16 GPa, higher than that of Ba_2MgH_6 (74.75 GPa), indicating greater rigidity and tensile strength. These values meet Born's stability criteria, confirming the structural stability of both materials even under extreme conditions [28].

Table 1. The computed results of elastic constants (C_{ij}) and Cauchy's pressure (C_P) of X_2MgH_6 (X=Ba, Sr)

C_{ij}	(Sr_2MgH_6) valeur (GPa)	(Ba_2MgH_6) valeur (GPa)
C_{11}	95.75525	84.82890
C_{12}	15.93295	14.05735
C_{13}	25.27545	19.02005
C_{33}	88.52470	72.78600
C_{44}	39.12120	31.87875
C_{66}	39.90955	35.29190
C_p	-23,18825	-17,8214

Table 2. (B), (G), (Y), (B/G), (G/B), (v), (H), and shear (A) calculated for the X_2MgH_6 (X=Ba, Sr)

compounds										
Compound	В	G	Y	B/G	G/B	θ	Н	A		
Sr_2MgH_6	45.940	37.169	87.16	1.23	0.80	0.18	7.93	0.98		
Ba_2MgH_6	38.653	31.737	74.753	1.21	0.82	0.18	6.75	0.90		

Mechanical module, which measure rigidity and resistance to deformation, further highlight this trend. From (4) to (9) were used to compute these module [53], [54]:

Bulk modulus (B):
$$B = \frac{(B_V + B_R)}{2}$$
 (4)

Shear modulus (G):
$$G = \frac{(G_V + G_R)}{2}$$
 (5)

Young's modulus (Y):
$$Y = \frac{9BG}{3B+G}$$
 (6)

Poisson's ratio (v):
$$v = \frac{3B-2G}{2(3B+G)}$$
 (7)

Microhardness (H):
$$H = \frac{(1-2\vartheta)Y}{6(1+\vartheta)}$$
 (8)

Zener anisotropy factor A: A =
$$\frac{2C_{44}}{C_{11}-C_{12}}$$
 (9)

Young's module, shear constants and Poisson's ratio for both materials are shown in Figures 6 and 7. Sr_2MgH_6 shows a shear modulus (G) of 37.17 GPa, higher than that of Ba_2MgH_6 (31.74 GPa), indicating better resistance to plastic deformation. This property is essential for applications where wear resistance and durability are paramount. In addition, Sr_2MgH_6 has a higher microhardness (7.93 vs. 6.75 for Ba_2MgH_6), which is advantageous for applications requiring increased wear resistance. However, the Pugh ratio (B/G≈1.2) and Cauchy pressure($C_{12} - C_{44} < 0$) classify these materials as brittle, typical of ceramics, with a dominance of ionic bonds (Poisson's ratio v=0.18).

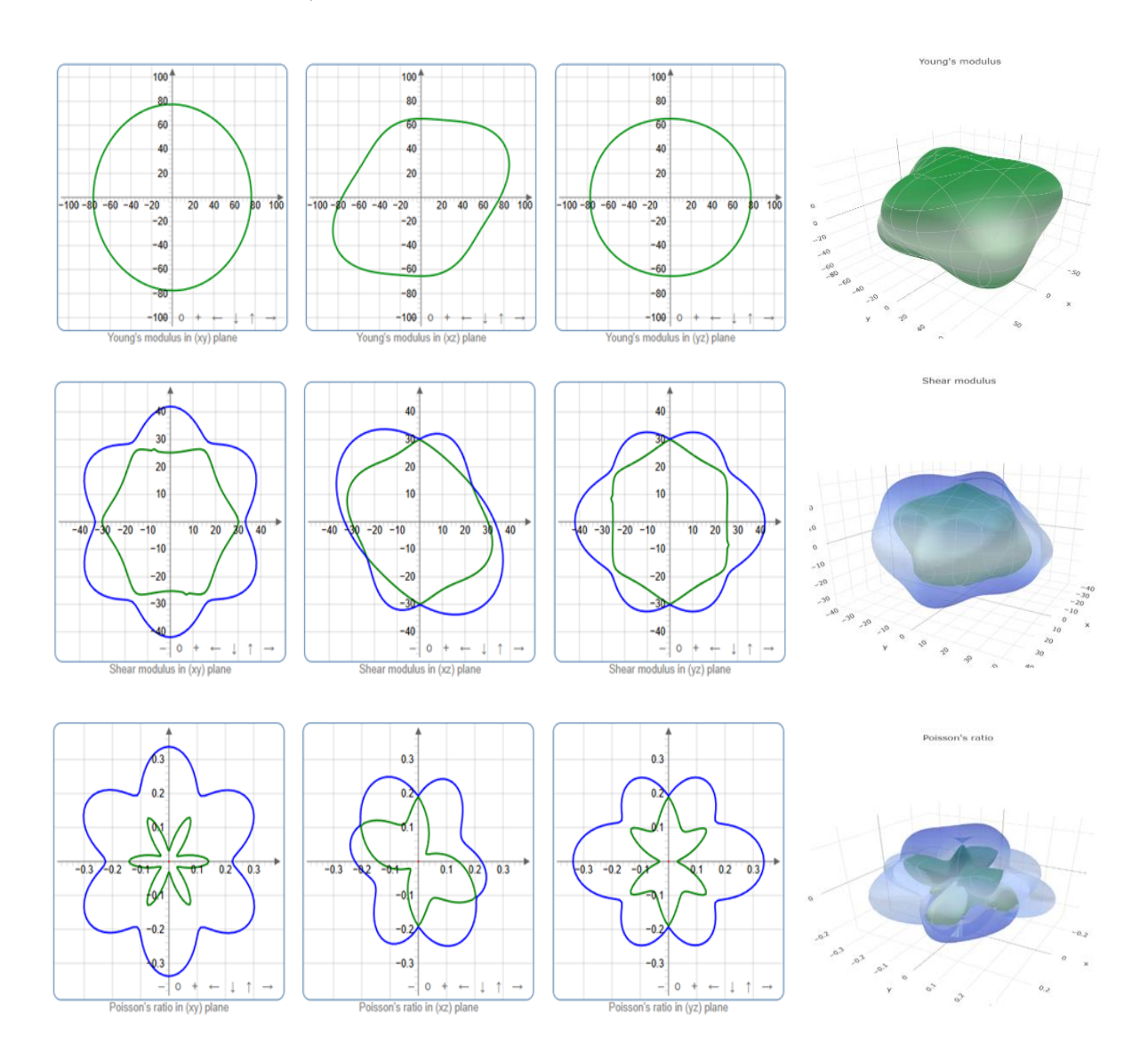


Figure 6. The young's modulus, shear constant and Poisson's ration of Ba_2MgH_6 are represented in 2D and

Figures 6 and 7 also show an almost isotropic mechanical response, which is advantageous for homogeneous manufacturing. These properties guide their applications: Sr_2MgH_6 , with its increased rigidity, is ideal for high-pressure vessels (700 bar), where resistance to cyclic stress is critical. Ba_2MgH_6 , although less effective in terms of rigidity, could be adapted to systems requiring a certain flexibility, such as separation membranes, thanks to its slightly higher G/B ratio (0.82 vs. 0.80 for Sr_2MgH_6).

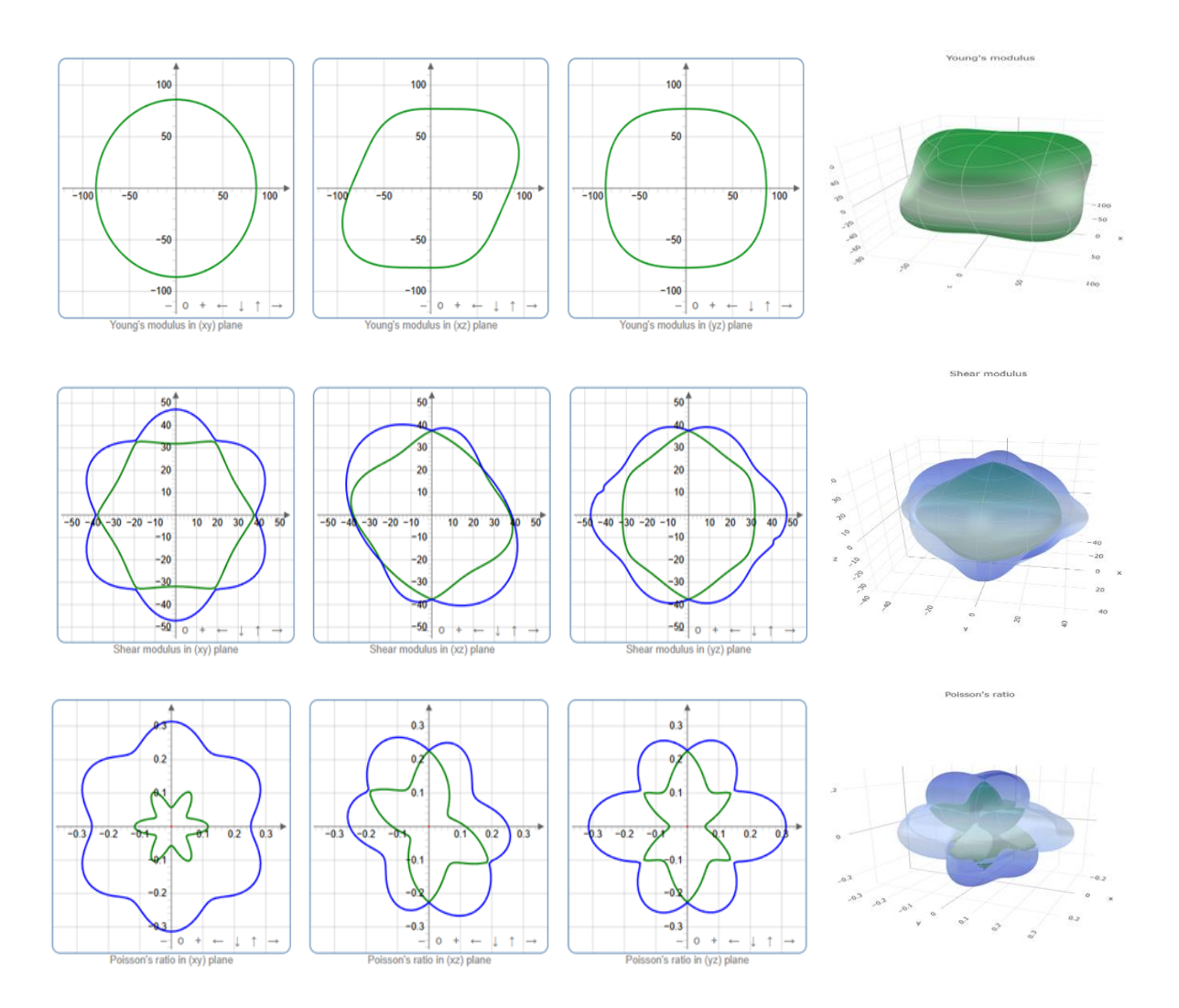


Figure 7. The young's modulus, shear constant and Poisson's ration of Sr_2MgH_6 are represented in 2D and 3D

Table 2 Shows the mass (B), (G), (Y), (B/G), (v), and (H) calculated for the two materials. The high values of this module for Sr_2MgH_6 confirm its mechanical superiority over Ba_2MgH_6 . For example, the (G) of 37.17 GPa for Sr_2MgH_6 indicates better resistance to shear deformation, essential for applications under high mechanical stress.

In conclusion, the mechanical properties of $Ba_2\text{Mg}H_6$ and $Sr_2\text{Mg}H_6$, highlighted in Figures 6 and 7 and Tables 1 and 2, show their potential for a variety of hydrogen storage applications. Compressive strength, stiffness and isotropic mechanical response are critical factors influencing the durability and performance of these materials. These insights are essential for optimizing these hydrides for more robust and durable energy storage technologies, paving the way for innovations in hydrogen storage materials [21], [55].

3.7. Optical properties

The Ba_2MgH_6 and Sr_2MgH_6 hydrides exhibit remarkable optical properties closely linked to their electronic structure and complex dielectric response [34], [35]:

$$\varepsilon(\omega) = \varepsilon_1(\omega) + i\varepsilon_2(\omega) \tag{10}$$

The hydrides $Ba_2 \text{Mg}H_6$ and $Sr_2 \text{Mg}H_6$ display remarkable optical properties, closely linked to their electronic structure and complex dielectric response. These optical characteristics pave the way for diverse applications in optoelectronics and photonics.

The refractive index, maximized at 2.5-3.0 eV for Sr_2MgH_6 versus 2.3 for Ba_2MgH_6 (Figures 8(a) and 8(b)), reveals enhanced light dispersion in the strontium compound. This property is particularly useful for waveguides or miniaturized photonic devices, where efficient light handling is essential.

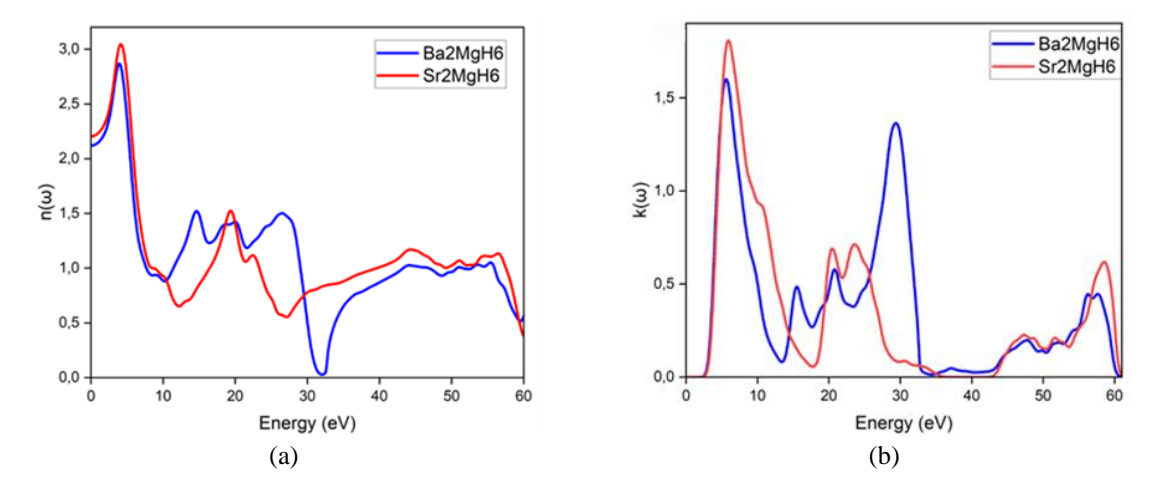


Figure 8. Optical properties of X_2 Mg H_6 (X=Ba, Sr): (a) refractive index n(ω) and (b) extinction coefficient k(ω)

The absorption mechanisms of these materials also show notable differences. As shown in Figure 9(a), Sr_2MgH_6 exhibits a sharp peak at 5.2 eV in the ultraviolet (UV), outperforming Ba_2MgH_6 (4.8 eV). This high UV absorption makes Sr_2MgH_6 promising for UV collectors or tandem solar cells. On the other hand, as illustrated in Figure 9(b), Ba_2MgH_6 exhibits reduced and more extensive infrared absorption, suggesting potential applications in optical telecommunications.

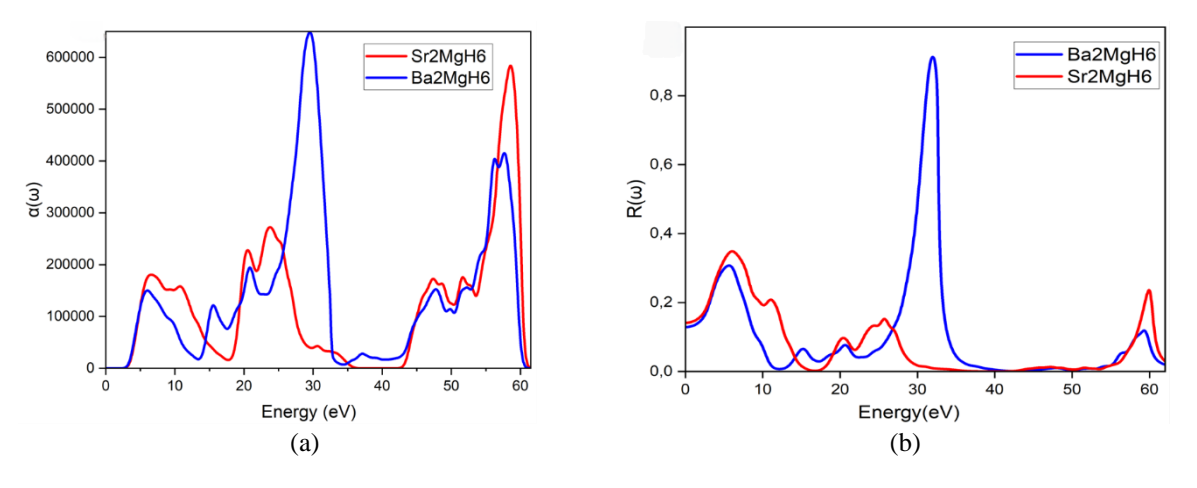


Figure 9. Optical characteristics of X_2 Mg H_6 (X=Ba, Sr): (a) absorption coefficient $\alpha(\omega)$ and (b) reflectivity $R(\omega)$

Dielectric functions, shown in Figures 10(a) and 10(b), highlight this optical duality. Sr_2MgH_6 shows high polarization ($\epsilon_1\approx20$) and optical loss peaks at 12 eV, indicating strong interaction with the electric field. These properties are ideal for dielectric applications and plasmonic sensors.

In contrast, Ba_2MgH_6 combines moderate metallicity (locally negative ε_1 values) and plasmonic resonances at 10 eV, making it suitable for metamaterials or high-sensitivity plasmonic sensors.

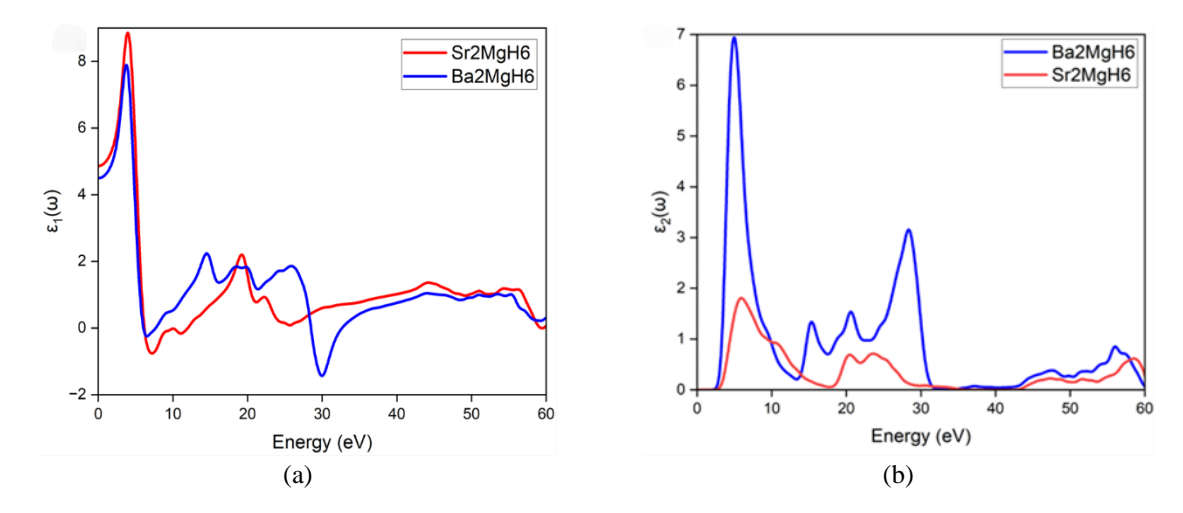


Figure 10. Dielectric functions of X_2 Mg H_6 (X=Ba, Sr): (a) the real part (ϵ_1) and (b) imaginary part (ϵ_2)

The optical conductivity spectra, shown in Figures 11(a) and 11(b), exhibit peaks at 4.6 eV and 10 eV, confirming subtle differences in the light–matter interaction between the two materials. Furthermore, the higher reflectivity of Sr_2MgH_6 in the visible region (45% compared to 35% for Ba_2MgH_6) suggests its potential use in anti-reflective coatings or selective mirror applications.

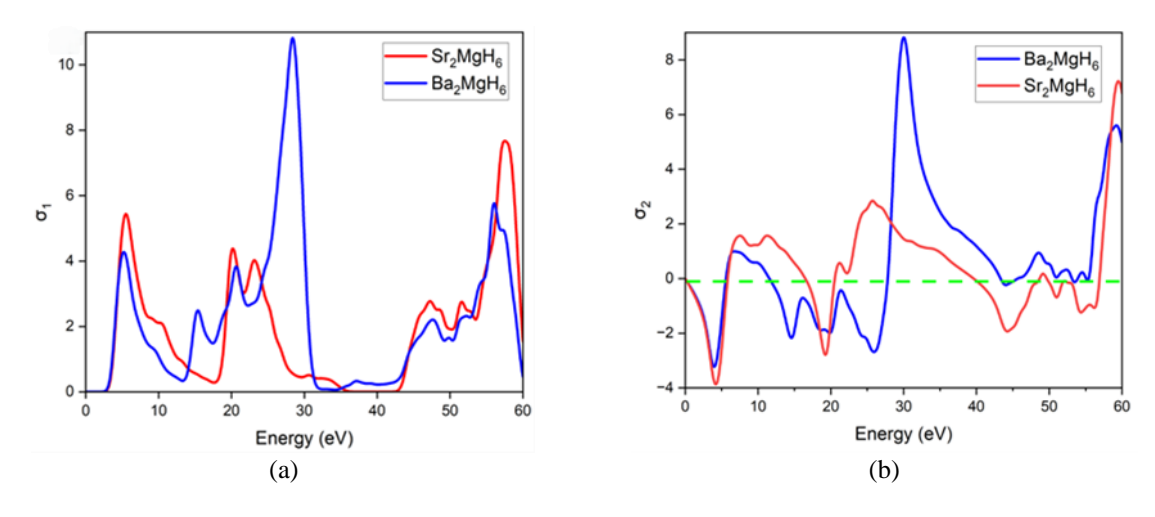


Figure 11. Optical conductivity of: (a) the real and (b) imaginary part

The $L(\omega)$ loss function, shown in Figure 12, is crucial for identifying plasmonic resonances. Sr_2MgH_6 shows optical loss peaks at 12 eV, indicating potential plasmonic resonances useful for plasmonic sensors. Ba_2MgH_6 shows resonances at 10 eV, suggesting similar applications but with slightly different characteristics.

Their structural stability and fluorescence potential, linked to crystal defects, could even revolutionize display technologies (LEDs, OLEDs) [36], [37]. Combining optical versatility and tunable performance, these hydrides form an innovative platform for optoelectronics and photonics. In-depth studies of their nonlinear effects and light emission mechanisms are needed to optimize their integration into advanced devices. These unique optical properties underline the potential of Ba_2MgH_6 and Sr_2MgH_6 for cutting-edge technological applications, contributing to the advancement of energy storage technologies and optical systems.

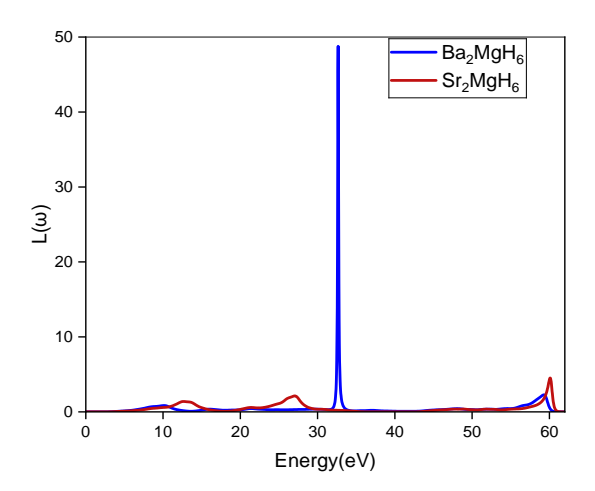


Figure 12. Loss function $L(\omega)$ for X_2MgH_6 (X = Ba, Sr)

4. CONCLUSION

This study elucidates the exceptional structural, electronic, mechanical, and optical characteristics of X_2 Mg H_6 (X=Ba, Sr) hydrides, positioning them as compelling candidates for advanced hydrogen storage systems. The double perovskite framework endows these materials with robust thermodynamic and mechanical stability, critical for enduring the cyclic stresses inherent in hydrogen storage applications. Electronic structure analyses reveal bandgap characteristics and DOS profiles that govern their semiconducting behavior and reactivity, while mechanical evaluations highlight their superior elastic moduli and hardness, particularly in Sr_2 Mg H_6 , underscoring their structural resilience. Optical investigations further demonstrate strong UV absorption and visible-spectrum reflectivity, suggesting potential utility in photonic and optoelectronic devices. By integrating these multifunctional properties, X_2 Mg H_6 hydrides emerge as versatile materials for energy-related technologies. However, targeted investigations into optimizing hydrogen desorption kinetics and tailoring thermodynamic parameters are imperative to bridge the gap between theoretical potential and industrial scalability. These findings advance the understanding of complex hydride systems and offer foundational insights for designing next-generation materials in sustainable energy storage and conversion, aligning with global imperatives for decarbonization and clean energy transition.

REFERENCES

- [1] T. Thomas, S. Bontha, A. Bishnoi, and P. Sharma, "MXene as a hydrogen storage material? a review from fundamentals to practical applications," *Journal of Energy Storage*, vol. 88, p. 111493, 2024, doi: 10.1016/j.est.2024.111493.
- [2] A. Q. Al-Shetwi, I. Z. Abidin, K. A. Mahafzah, and M. A. Hannan, "Feasibility of future transition to 100% renewable energy: recent progress, policies, challenges, and perspectives," *Journal of Cleaner Production*, vol. 478, p. 143942, Jan. 2024, doi: 10.1016/j.jclepro.2024.143942.
- [3] M. Filonchyk et al., "Greenhouse gas emissions and reduction strategies for the world's largest greenhouse gas emitters," Science of The Total Environment, vol. 944, p. 173895, Jan. 2024, doi: 10.1016/j.scitotenv.2024.173895.
- [4] P. Moriarty and D. Honnery, "What is the global potential for renewable energy?," Renewable and Sustainable Energy Reviews, vol. 16, no. 1, pp. 244–252, Jan. 2012, doi: 10.1016/j.rser.2011.07.151.
- [5] L. Mulky et al., "An overview of hydrogen storage technologies key challenges and opportunities," *Materials Chemistry and Physics*, vol. 325, p. 129710, Oct. 2024, doi: 10.1016/j.matchemphys.2024.129710.
- [6] M. M. Rampai, C. B. Mtshali, N. S. Seroka, and L. Khotseng, "Hydrogen production, storage, and transportation: recent advances," RSC Adv, vol. 14, no. 10, pp. 6699–6718, 2024, doi: 10.1039/D3RA08305E.
- [7] A. Miled, S. Mellouli, H. B. Maad, and F. Askri, "Improvement of the performance of metal hydride pump by using phase change heat exchanger," *International Journal of Hydrogen Energy*, vol. 42, no. 42, pp. 26343–26361, 2017, doi: 10.1016/j.ijhydene.2017.08.118.
- [8] Y. J. Wang et al., "Improving fatigue performance of cr-coated zirconium alloy cladding by ultrasonic shot-peening proces," Journal of Materials Research and Technology, vol. 27, no. October, pp. 6047–6057, 2023, doi: 10.1016/j.jmrt.2023.11.102.
- [9] B. Rezaie and M. A. Rosen, "District heating and cooling: review of technology and potential enhancements," Applied Energy, vol. 93, pp. 2–10, 2012, doi: 10.1016/j.apenergy.2011.04.020.
- [10] R. Murphy, "What is undermining climate change mitigation? how fossil-fuelled practices challenge low-carbon transitions," Energy Research and Social Science, vol. 108, p. 103390, 2024, doi: 10.1016/j.erss.2023.103390.
- [11] B. S. Zainal et al., "Recent advancement and assessment of green hydrogen production technologies," Renewable and Sustainable Energy Reviews, vol. 189, p. 113941, 2024, doi: 10.1016/j.rser.2023.113941.
- [12] S. Hossain, N. Islam, K. Shariar, M. M. Hasan, and S. Hossain, "The role of solar thermal hydrogen production technologies in future energy solutions: a review," *Energy Conversion and Management: X*, p. 100876, Jan. 2025, doi: 10.1016/j.ecmx.2025.100876.
- [13] Y. Xu, Y. Zhou, Y. Li, and Z. Ding, "Research progress and application prospects of solid-state hydrogen storage technology,"

- Molecules, vol. 29, no. 8, 2024, doi: 10.3390/molecules29081767.
- [14] A. M. Jodeiri, M. J. Goldsworthy, S. Buffa, and M. Cozzini, "Role of sustainable heat sources in transition towards fourth generation district heating - a review," Renewable and Sustainable Energy Reviews, vol. 158, 2022, doi: 10.1016/j.rser.2022.112156.
- [15] J. O. Abe, A. P. I. Popoola, E. Ajenifuja, and O. M. Popoola, "Hydrogen energy, economy and storage: review and recommendation," International Journal of Hydrogen Energy, vol. 44, no. 29, pp. 15072-15086, 2019, doi: /10.1016/j.ijhydene.2019.04.068.
- [16] M. Nasser, T. F. Megahed, S. Ookawara, and others, "A review of water electrolysis-based systems for hydrogen production using hybrid/solar/wind energy systems," Environmental Science and Pollution Research, vol. 29, pp. 86994-87018, 2022, doi: 10.1007/s11356-022-23323-y.
- R. Song et al., "Insight into the mechanical, electronic, kinetic, thermodynamic, and hydrogen storage properties of xfeh3 (x=ca, sr, ba) perovskites for hydrogen storage applications: first-principle calculations," Chinese Journal of Physics, vol. 89, pp. 1152-1163, 2024, doi: 10.1016/j.cjph.2023.12.040.
- M. P. Limsi et al., "Conception et intégration d'un stockage d'hydrogène sur hydrures métalliques thèse," PhD Thesis, 2008.
- S. Li, L. Zhang, F. Wu, Y. Jiang, and X. Yu, "Efficient catalysis of fenicu-based multi-site alloys on magnesium-hydride for solid-state hydrogen storage," Chinese Chemical Letters, vol. 36, no. 1, p. 109566, Jan. 2025, doi: 10.1016/j.cclet.2024.109566.
- Q. Dai, Q. Q. Liang, T. Y. Tang, H. X. Gao, S. Q. Wu, and Y. L. Tang, "Insights on structural, elastic, electronic, optical and thermodynamic properties and population analysis of double perovskite oxide ba2mgxo6 (x = se, te)," Materials Science in Semiconductor Processing, vol. 171, 2023, p. 108003, 2024, doi: 10.1016/j.mssp.2023.108003.
- Q. Dai, T. Y. Tang, Q. Q. Liang, Z. Q. Chen, Y. Wang, and Y. L. Tang, "Exploration of a2bh6(a = k, rb; b = ge, sn) hydrides for hydrogen storage applications: a first principles study," International Journal of Hydrogen Energy, vol. 92, pp. 769-778, 2024, doi: 10.1016/j.ijhydene.2024.10.324.
- M. Mubashir, M. Ali, M. Yousaf, H. Huang, and M. J. I. Khan, "Exploring promising kah3 (a = ca, sr and ba) hydrides for solidstate hydrogen storage and thermoelectric applications," International Journal of Hydrogen Energy, vol. 82, pp. 1435–1445, Jan. 2024, doi: 10.1016/j.ijhydene.2024.08.029.
- G. Surucu, A. Candan, A. Gencer, and M. Isik, "First-principle investigation for the hydrogen storage properties of naxh3 (x= mn, fe, co) perovskite type hydrides," International Journal of Hydrogen Energy, vol. 44, no. 57, pp. 30218-30225, 2019, doi: 10.1016/j.ijhydene.2019.09.201.
- S. Al and Ç. Yamçıçıer, "Computational exploration of hexahydride materials (k2sih6 and rb2sih6); structural, mechanical, thermodynamic, optic, electronic and dynamic properties," Journal of Energy Storage, vol. 91, 2024, doi: 10.1016/j.est.2024.112033.
- W. Kohn, A. D. Becke, and R. G. Parr, "Density functional theory of electronic structure," The Journal of Physical Chemistry, vol. 100, no. 31, pp. 12974–12980, Jan. 1996, doi: 10.1021/jp9606691.
- [26] M. B. Kanoun, S. Goumri-Said, and K. Abdullah, "8 theoretical study of physical properties and oxygen incorporation effect in nanolaminated ternary carbides 211-max phases," in *Advances in Science and Technology of Mn+1AXn Phases*, I. M. Low, Ed., Woodhead Publishing, 2012, pp. 177-196.
- "CASTEP guide." Dassault Systèmes Customer Support, Jan. 2024.
 S. J. Clark *et al.*, "First principles methods using castep," *Zeitschrift für Kristallographie Crystalline Materials*, vol. 220, no. 5– 6, pp. 567-570, Jan. 2005, doi: 10.1524/zkri.220.5.567.65075.
- [29] A. Siddique et al., "Structures and hydrogen storage properties of aevh3 (ae = be, mg, ca, sr) perovskite hydrides by dft calculations," International Journal of Hydrogen Energy, vol. 48, no. 63, pp. 24401-24411, Jan. 2023, doi: 10.1016/j.ijhydene.2023.03.139.
- A. Benghia, T. Dahame, and B. Bentria, "First principle calculation of physical properties of barium based chalcogenides bam4s7 (m = ga, al); a dft, dft-d and hybrid functional hse06 study," Optical Materials, vol. 54, pp. 269-275, 2016, doi: 10.1016/j.optmat.2016.02.027.
- [31] Ç. Yamçıçıer, "Exploring the structural, elastic, phonon, optoelectronics, and thermoelectric properties of tetragonal complex metal hydride x2mgh4 (x=k, rb, and cs) compounds for hydrogen storage applications," International Journal of Hydrogen Energy, vol. 48, no. 100, pp. 39930-39943, Jan. 2023, doi: 10.1016/j.ijhydene.2023.09.177.
- [32] G. Barone, A. Buonomano, C. Forzano, and A. Palombo, "A novel dynamic simulation model for the thermo-economic analysis and optimisation of district heating systems," Energy Conversion and Management, vol. 220, p. 113052, 2020, doi: 10.1016/j.enconman.2020.113052.
- [33] M. Archi, O. Bajjou, k. Rahmani, and B. Elhadadi, "A comparative ab initio analysis of the stability, electronic, thermodynamic, mechanical, and hydrogen storage properties of srznh3 and srlih3 perovskite hydrides through dft and aimd approaches," International Journal of Hydrogen Energy, vol. 105, pp. 759-770, Jan. 2025, doi: 10.1016/j.ijhydene.2025.01.312.
- M. Born, "On the stability of crystal lattices. i," Mathematical Proceedings of the Cambridge Philosophical Society, vol. 36, no. 2, pp. 160–172, Jan. 1940, doi: 10.1017/S0305004100017138.
- F. Sciences and U. M. V-rabat, "Centre d'etudes doctorales sciences et technologies," vol. 00212, no. 05, 2022.
- [36] M. mana Al-Anazy et al., "Study of alkaline metals hydrides rbxh3 (x = mg/ca/sr/ba) for green energy and hydrogen storage applications," International Journal of Hydrogen Energy, vol. 78, pp. 927-937, Jan. 2024, doi: 10.1016/j.ijhydene.2024.06.373.
- G. Gondor, "Pour le stockage de l'hydrogène : analyse thermodynamique de la formation d'hydrures métalliques et optimisation du remplissage d'un réservoir.," p. 181, 2013.
- G. M. Mustafa *et al.*, "Study of structural, optical, mechanical, thermoelectric, and hydrogen storage properties of csxh3 (x = ca, sr, ba) hydrides," *International Journal of Hydrogen Energy*, vol. 92, pp. 938–948, Jan. 2024, doi: 10.1016/j.ijhydene.2024.10.245.
- R. Song, N. Xu, Y. Chen, S. Chen, W. Dai, and W. Zhang, "First-principles investigation for the hydrogen storage, mechanical, electronic, optical, dynamic, and thermodynamic properties of xmnh3 (x=na, k, rb) perovskites for hydrogen storage applications," Vacuum, vol. 222, p. 113007, 2024, doi: 10.1016/j.vacuum.2024.113007.
- M. K. Shahzad et al., "Computational study of rubidium-rb based cubic rb2tlcof6 double perovskite material for photocatalytic water degradation applications: a dft investigations," International Journal of Hydrogen Energy, vol. 89, pp. 117-126, Jan. 2024, doi: 10.1016/j.ijhydene.2024.09.305.
- G. M. Mustafa et al., "First principle study of physical aspects and hydrogen storage capacity of magnesium-based double perovskite hydrides mg2xh6 (x = cr, mn)," International Journal of Hydrogen Energy, vol. 95, pp. 300-308, Jan. 2024, doi: 10.1016/j.ijhydene.2024.11.112.
- J. Li et al., "Small-scale high-pressure hydrogen storage vessels: a review," Materials, vol. 17, no. 3, 2024, doi: [42] 10.3390/ma17030721.

[43] X. He *et al.*, "Excellent microwave absorption performance of lafeo3/fe3o4/c perovskite composites with optimized structure and impedance matching," *Carbon*, vol. 213, p. 118200, 2023, doi: 10.1016/j.carbon.2023.118200.

- [44] M. Umer et al., "First principles investigation of structural, mechanical, thermodynamic, and electronic properties of al-based perovskites xalh3 (x=k, rb, cs) for hydrogen storage," *International Journal of Hydrogen Energy*, vol. 61, pp. 820–830, Jan. 2024, doi: 10.1016/j.ijhydene.2024.02.333.
- [45] S. Bahou, H. Labrim, M. Lakhal, M. Bhihi, B. Hartiti, and H. Ez-Zahraouy, "Improving desorption temperature and kinetic properties in mgh2 by vacancy defects: dft study," *International Journal of Hydrogen Energy*, vol. 45, no. 18, pp. 10806–10813, Jan. 2020, doi: 10.1016/j.ijhydene.2020.02.024.
- [46] G. Bianchi *et al.*, "Development and analysis of a packaged trilateral flash cycle system for low grade heat to power conversion applications," *Thermal Science and Engineering Progress*, vol. 4, pp. 113–121, 2017, doi: 10.1016/j.tsep.2017.09.009.
- [47] Y. Ye, J. Lu, J. Ding, W. Wang, and J. Yan, "Performance improvement of metal hydride hydrogen storage tanks by using phase change materials," *Applied Energy*, vol. 320, p. 119290, 2022, doi: 10.1016/j.apenergy.2022.119290.
- [48] M. A. Rahman et al., "Comparative analysis of kxh3(x= mg, be) hydride cubic perovskites for hydrogen storage properties: a computational approach," International Journal of Hydrogen Energy, vol. 80, pp. 725–732, 2024, doi: 10.1016/j.ijhydene.2024.07.064.
- [49] L. U. D. E. Bordeaux, É. Doctorale, D. E. S. Sciences, S. P. D. E. La, M. Condensee, and E. L. U. Libanaise, "L'université de bordeaux," 2014.
- [50] A. Izanlou and M. K. Aydinol, "An ab initio study of dissociative adsorption of h2 on feti surfaces," *International Journal of Hydrogen Energy*, vol. 35, no. 4, pp. 1681–1692, 2010, doi: 10.1016/j.ijhydene.2009.12.136.
- [51] K. D. Ćirić *et al.*, "A study on crystal structure, bonding and hydriding properties of ti–fe–ni intermetallics–behind substitution of iron by nickel," *international journal of hydrogen energy*, vol. 37, no. 10, pp. 8408–8417, 2012.
- [52] W. Zhou et al., "CoSe2 nanoparticles embedded defective carbon nanotubes derived from mofs as efficient electrocatalyst for hydrogen evolution reaction," Nano Energy, vol. 28, pp. 143–150, 2016, doi: 10.1016/j.nanoen.2016.08.040.
- [53] W. Zheng, F. S. Liu, Y. C. Lu, Z. T. Liu, W. H. Liu, and Q. J. Liu, "First-principles calculations of the structural, mechanical, electronic, and optical properties of bax2 (x=0, s, se and te) compounds," *Materials Science in Semiconductor Processing*, vol. 147, no. March, p. 106755, 2022, doi: 10.1016/j.mssp.2022.106755.
- [54] M. A. Ali, M. M. Hossain, A. K. M. A. Islam, and S. H. Naqib, "Ternary boride hf3pb4: insights into the physical properties of the hardest possible boride max phase," *Journal of Alloys and Compounds*, vol. 857, p. 158264, 2021, doi: 10.1016/j.jallcom.2020.158264.
- [55] J. Wu, B. Zhang, and Y. Zhan, "Explorations on tiosx (x=b, c, n, o and si) alloys for potential superhard materials from first-principle calculation," *Journal of Physics and Chemistry of Solids*, vol. 104, 2016, pp. 207–213, 2017, doi: 10.1016/j.jpcs.2017.01.025.